A vesicle-to-sponge transition via the proliferation of membrane-linking pores in w-3 polyunsaturated fatty acid-containing lipid assemblies

Angelina Angelova, Borislav Angelov, Vasil M Garamus, Markus Drechsler

▶ **To cite this version:**

Angelina Angelova, Borislav Angelov, Vasil M Garamus, Markus Drechsler. A vesicle-to-sponge transition via the proliferation of membrane-linking pores in w-3 polyunsaturated fatty acid-containing lipid assemblies. Journal of Molecular Liquids, 2019, 279, pp.518-523. 10.1016/j.molliq.2019.01.124 . hal-02381509

HAL Id: hal-02381509
https://hal.science/hal-02381509v1

Submitted on 26 Nov 2019

HAL is a multi-disciplinary open access archive for the deposit and dissemination of scientific research documents, whether they are published or not. The documents may come from teaching and research institutions in France or abroad, or from public or private research centers.

L'archive ouverte pluridisciplinaire **HAL**, est destinée au dépôt et à la diffusion de documents scientifiques de niveau recherche, publiés ou non, émanant des établissements d'enseignement et de recherche français ou étrangers, des laboratoires publics ou privés.

A vesicle-to-sponge transition *via* the proliferation of membrane-linking pores in ω-3 polyunsaturated fatty acid-containing lipid assemblies

Angelina Angelova[a], Borislav Angelov[b,]*, Vasil M. Garamus[c], Markus Drechsler[d]

[a]Institut Galien Paris-Sud, CNRS UMR 8612, Univ. Paris-Sud, LabEx LERMIT, Univ Paris-Saclay, F-92290 Châtenay-Malabry cedex, France

[b]Institute of Physics, ELI Beamlines, Academy of Sciences of the Czech Republic, Na Slovance 2, CZ-18221 Prague, Czech Republic,

[c]Helmholtz-Zentrum Geesthacht: Centre for Materials and Coastal Research, D-21502 Geesthacht, Germany ,

[d]Keylab "Electron and Optical Microscopy", Bavarian Polymerinstitute (BPI), University of Bayreuth, D-95440 Bayreuth, Germany,

* Corresponding author: Borislav.Angelov@eli-beams.eu

Authors ORCID ID:
Angelina Angelova: 0000-0002-0285-0637
Borislav Angelov: 0000-0003-3131-4822
Vasil M. Garamus: 0000-0001-9315-4188
Markus Drechsler: 0000-0001-7192-7821

Highlights

- Mixed membrane assemblies of monoolein and a ω-3 polyunsaturated fatty acid characterized by non-trivial porous topologies
- Amphiphilic composition-triggered transition from a vesicle to a sponge structure at room temperature
- Small-angle X-ray scattering (SAXS) patterns detect the internal nanostructure transformation due to curvature changes
- Cryo-TEM imaging reveals a sequence of intermediate states upon the vesicle-to-sponge nanoparticle transition

Abstract

We investigate the nanostructure evolution and the membrane reorganization of diluted lipid dispersions of self-assembled monoolein (MO)/eicosapentaenoic acid (EPA, 20:5) mixtures by synchrotron small-angle X-ray scattering (SAXS) and cryogenic transmission electron microscopy (cryo-TEM) microscopy. The nonlamellar lipid phase containing a ω-3 polyunsaturated fatty acid was fragmented into stable nanoscale objects with the help of PEGylated lipids. The Cryo-TEM imaging revealed the transformation pathway of the vesicular bilayer membranes into sponge nanoparticles (spongosomes) in excess aqueous medium. At ambient temperature, the topological transition occurred through the proliferation of membrane-linking pores (MLP) within the individual lipid nanoparticles. The density of the MLP pores varied starting from the nanoparticle center towards the periphery. The generation of MLP is governed by the amphiphilic composition and leads to formation of 3D networks of aqueous channels inside the nanoparticles, *i.e.* spongosomes. A higher density of MLP pores was established at increasing fraction of EPA in the mixed lipid membranes. This corresponded to sponge particles of less hydrated internal structure, *i.e*. with smaller-size aqueous compartments. Synchrotron SAXS patterns characterized the overall structural transition from vesicles to sponge membranes in the studied lipid systems. It can be concluded that the incorporation of a ω-3 polyunsaturated fatty acid at increasing concentration causes swelling inhibition (dehydration) of the host liquid crystalline architectures.

Graphical abstract

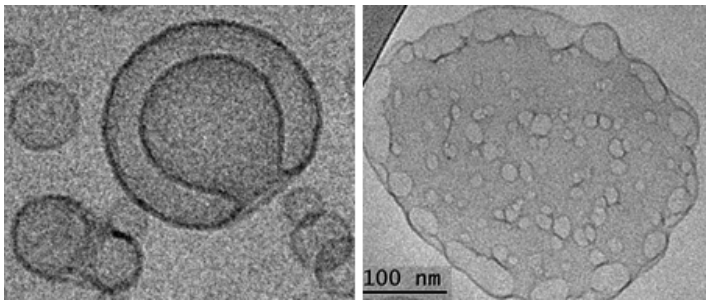

Cryo-TEM images of composition-induced intermediate structural states upon a vesicle-to-sponge membrane transition

Keywords

- membrane curvature,
- vesicle,
- spongosome,
- mesophase transition,
- swelling inhibition,
- BioSAXS

1. Introduction

The phase transitions between lyotropic liquid crystalline states [1-3] of synthetic lipid membranes have broad applications in many fields, for instance in the crystallization of proteins and other bioactive compounds, the encapsulation of genetic material, the development of drug delivery systems and carriers for the protection of instable dyes, diagnostic agents, or food ingredients [4-20]. Significant progress in the understanding of the involved structural mechanisms can be achieved by the small-angle X-ray scattering (SAXS) method [21-28]. The analysis of the synchrotron X-ray scattering patterns has seldom been accompanied by local inspection of the samples by direct cryo-TEM microscopy imaging [29-34]. In several cases, coexisting or intermediate types of liquid crystalline structures have been detected among the lamellar, bicontinuous cubic, inverted hexagonal and sponge phases [7,22-26,35-37].

Liquid crystalline phase transformations of membranous assemblies are triggered by lipid monolayer curvature changes due to (i) the modifications of the degree of lipid hydration (concentration-driven transitions), (ii) the incorporation of co-lipids and hydrophobic guest molecules in the lipid bilayers or binding of soluble peptides (or other substances) at the membrane surface (composition-driven transitions), (iii) the biochemical processes (*e.g.* lipid oxidation, lipid hydrolysis, and other enzymatic reactions), or (iv) the application of environmental stimuli (temperature jumps, exposure to light, pressure, electrostatic effects, pH, *etc*) [2-4,38-41]. The molecular compositions, determining the properties of the lipid and amphiphile mixtures (lipid molecular shape, chain length, chain saturation, asymmetry of the hydrophobic moieties, headgroup polarity and size), govern the interfacial curvature and the elastic properties of the obtained membrane assemblies. Intermediate phases of unusual topologies and/or hierarchical organizations have been observed in amphiphilic systems of multicomponent compositions [42-44]. For instance, "mesh" phases have been reported with ternary self-assembled systems consisting of a nonionic surfactant, oil, and water [44]. The mesh phase is an example of an intermediate phase built-up by perforated lamellas.

Lamellar-to-cubic and lamellar-to-sponge phase transitions present current interest from both theoretical and experimental view points [45-51]. Four major axes of previous research on the topology and the mechanism of such liquid crystalline phase transitions can be highlighted:

(a) Scaling of sponge phases as a function of the hydration level, which results in swelling of the aqueous channels and a solvent-dependent variation of the intermembrane distances [52-55].

(b) Topology evolution and kinetic trapping of non-spherical, folded or fluctuating vesicular superstructures as a function of the sample preparation and the conditioning methods (extrusion, sonication, shaking, annealing, quenching, *etc*.) [56-60].

(c) Pathway and kinetics of thermally-inducible liquid crystalline phase transitions between lamellar, cubic or sponge phases with a focus on the intermediate states [61-67].

(d) Composition-induced liquid crystalline phase transitions upon inclusion of curvature-modulating agents at room temperature [68-72].

Theoretical modelling studies of lipid vesicles of non-trivial topologies have considered the perforated vesicles as high genus topologies [73-75]. Scheme 1 displays the geometries corresponding to membrane linking pores (MLP), "necks" and enlarged pores. Shape transformations in high genus vesicles are assumed to occur through the proliferation of membrane linking pores (MLP). This assumption requires a direct experimental evidence for the case of multi-component synthetic lipid systems.

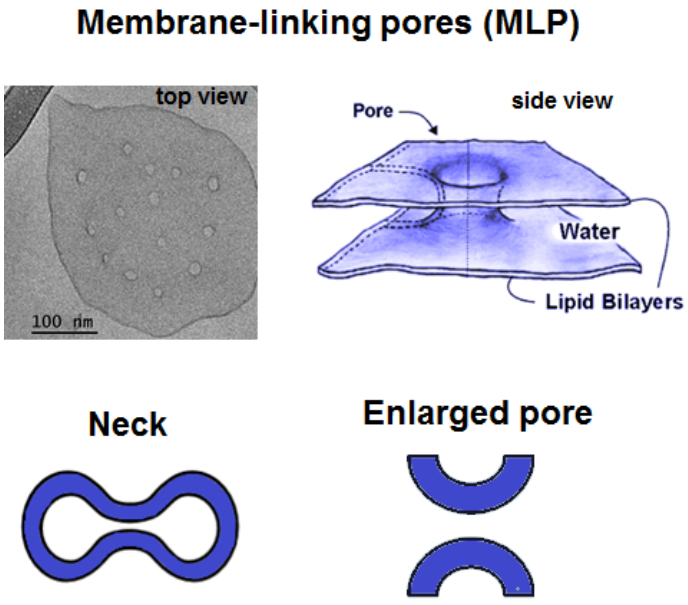

Scheme 1. Top and side view of membrane linking pores (MLP) and models of "necks" and enlarged pores formed by bilayer lipid membranes.

In the present work, we focus on the vesicle-to-sponge membrane topological transition, which is triggered by tuning of the lipid monolayer curvature in mixed liquid crystalline

structures of the nonlamellar lipid monoolein (MO) and the ω-3 polyunsaturated fatty acid EPA (eicosapentaenoic acid, 20:5). We use synchrotron small-angle X-ray scattering (SAXS) to assess the internal nanostructure transformation in the mixed lipid assemblies dispersed by sonication. Cryogenic transmission electron microscopy (Cryo-TEM) reveals the nanoscale features of the vesicle-to-sponge liquid crystalline phase transition, and in particular, the kinetically trapped intermediate stages of the self-assembly process.

2. Materials and methods

2.1. Materials and sample preparation

Powder of 1-monooleoyl-*rac*-glycerol (MO) [C18:1c9, MW 356.54, purity 99.5%], *cis*-5,8,11,14,17 eicosapentaenoic acid (20:5, EPA), and D-α-tocopherol polyethylene glycol 1000 succinate ($TPGS_{1000}$) were purchased from *Sigma-Aldrich* (France). The phospholipid *1,2*-dioleoyl-*sn*-glycero-*3*-phosphoethanolamine-*N*-(methoxy(polyethyleneglycol)-2000) ammonium salt (DOPE-PEG_{2000}) (M_W 2801.51 g/mol) was purchased from *Avanti Polar Lipids* (*Coger*, Paris, France). A phosphate buffer solution (NaH_2PO_4/Na_2HPO_4, 1.10^{-2}M, pH 7, p.a. grade, *Merck*) was prepared using Milli-Q water (*Millipore Co*.). It contained a small quantity of the antioxidant butylated hydroxytoluene (BHT).

Self-assembled bulk MO/EPA mixtures were dispersed into liquid crystalline nanoparticles by the method of hydration of a dry lipid film followed by physical agitation. First, chloroform solutions of MO and EPA were mixed at different ratios from 85/15 to 30/70 (mol/mol). The PEGylated lipid component was added at a constant percentage (3 mol.% with regard to MO). After mixing of the amphiphiles, the solvent was evaporated from the MO/EPA/DOPE-PEG_{2000} and MO/EPA/$TPGS_{1000}$ samples under a gentle stream of nitrogen gas in order to obtain fine and homogeneous lipid films. The latter were lyophilized overnight. The hydration of the mixed lipid layers was performed by incubation with a BHT-containing phosphate buffer solution at room temperature. Nanoparticulate dispersions were obtained in 95wt.% excess aqueous phase by vortexing and agitation in an ice bath. Ultrasonic cycles with a total duration of about 20 minutes (Branson 2510 ultrasonic bath, "set sonics" mode, power 60W) were performed.

2.2. Synchrotron SAXS measurements

Synchrotron SAXS experiments were performed at the P12 BioSAXS beamline [76] of the European Molecular Biology Laboratory (EMBL) at the storage ring PETRA III of the Deutsche Elektronen Synchrotron (DESY, Hamburg, Germany) at 20 °C using a Pilatus 2M detector (1475 x 1679 pixels) (Dectris, Switzerland) and synchrotron radiation with a wavelength λ = 0.1 nm. The sample-to-detector distance was 3 m, allowing for measurements in the q-range interval from 0.1 to 4.4 nm^{-1}. The q-vector was defined as $q = (4\pi/\lambda) \sin \theta$,

where 2θ is the scattering angle. The *q*-range was calibrated using the diffraction patterns of silver behenate. The experimental data were normalized with respect to the transmitted beam intensity and corrected for non-homogeneous detector response. The background scattering of the quartz capillary and the aqueous buffer was subtracted. The aqueous buffer scattering was measured before and after every sample scattering in order to control for eventual sample holder contamination. Twenty consecutive frames (each 0.05 sec) comprising the measurements for the sample and the solvent were acquired. No measurable radiation damage was detected by the comparison of the frames. The final scattering curve was obtained using the program PRIMUS [77] by averaging the scattering data collected from the different frames. An automatic sample changer adjusted for sample volume of 20 μL and a filling cycle of 60 sec was used.

2.3. Cryogenic Transmission Electron Microscopy (Cryo-TEM)

For cryo-TEM studies, a sample droplet of 2μL was put on a lacey carbon film covered copper grid (Science Services, Munich, Germany), which was hydrophilized by glow discharge (Solarus, Gatan, Munich, Germany) for 30s. Most of the liquid was then removed with blotting paper, leaving a thin film stretched over the lace holes. The specimen was instantly shock frozen by rapid immersion into liquid ethane and cooled to approximately 90 K by liquid nitrogen in a temperature-and humidity controlled freezing unit (Leica EMGP, Wetzlar, Germany). The temperature and humidity were monitored and kept constant in the chamber during all sample preparation steps. The specimen was inserted into a cryo transfer holder (CT3500, Gatan, Munich, Germany) and transferred to a Zeiss EM922 Omega energy-filtered TEM (EFTEM) instrument (Carl Zeiss Microscopy, Jena, Germany). Examinations were carried out at temperatures around 90 K. The TEM instrument was operated at an acceleration voltage of 200 kV. Zero-loss-filtered images (DE = 0 eV) were taken under reduced dose conditions (100-1000 e/nm^2). The images were recorded digitally by a bottom-mounted charge-coupled device (CCD) camera system (Ultra Scan 1000, Gatan, Munich, Germany) and combined and processed with a digital imaging processing system (Digital Micrograph GMS 1.9, Gatan, Munich, Germany). The sizes of the investigated nanoparticles were in the range or below the film thickness and no deformations were observed. The images were taken very close to focus or slightly under the focus (some nanometers) due to the contrast enhancing capabilities of the in-column filter of the employed Zeiss EM922 Omega. In EFTEMs, deep underfocused images can be totally avoided.

3. Results and discussion

3.1. Small angle X-ray scattering (SAXS) patterns revealing structural intermediates of the vesicle-to-sponge nanoparticle transition

The SAXS patterns of the diluted MO/EPA nanoparticle dispersions are presented in Figure 1a. They reveal that the ω-3 polyunsaturated fatty acid EPA modifies the organization of the MO lipid membranes and their propensity for ordering into periodic 3D assemblies (cubosomes or multilamellar lipid particles). Neither well-defined Bragg diffraction peaks nor scattering of a unique single population of vesicles were detected under the investigated dispersion conditions of the self-assembled mixtures. The observed scattering from the diluted MO/EPA/$TPGS_{1000}$ mixture, which involves a low EPA molar percentage (Fig. 1a, blue plot), may arise from coexisting double bilayer vesicles, unilamellar vesicles, and precursors of cubosome or spongosome particles with inner liquid crystalline structures [70].

Figure 1b presents a theoretical SAXS plot obtained with a scattering model for double membrane vesicles characterized by a random distribution [78] of the thickness of the aqueous compartments. A best match with the shape of the experimental SAXS curve (Figure 1a, blue plot) was found for the double-bilayer-vesicle model shown in Figure 1b (inset), for which the inner vesicle radius, R, was 100 nm and the lipid bilayer thickness was 2.3 nm. Thus, the bump centred at a scattering vector $q \approx 0.3$ nm^{-1} can be ascribed to the form factor resulting from a mixture of double bilayer vesicles with a random distribution of the aqueous domain thickness (*i.e*. the thickness of the aqueous buffer solvent, t_{sol}, between the membranes). The qualitative comparison of the modelled SAXS pattern (Figure 1b) with the experimental one (Figure 1a) indicated that the bumps observed at $q \approx 0.16$ and 0.3 nm^{-1} are common main features for both the experimental and the modelled scattering curves. Lipid nanoparticle topologies of a double-bilayer membrane type are shown in Figure 2 (top left panel) and Figure 3 (left panel) below.

The broad scattering maximum at $q \approx 1.55$ nm^{-1} (Fig. 1a, red plot) can be ascribed to the formation of sponge lipid nanoparticles as the major nanoparticles population in the EPA-rich dispersion (MO/EPA ratio 30/70 mol/mol). Such topologies are shown in Figure 3 (right panel). The corresponding correlation distances at $q = 2\pi/d \approx 1.55$ nm^{-1} were estimated to be $d \approx 4$ nm. Such distances are typical for oil-rich sponges with a low hydration domain between the bilayer membranes. The scattering detected at the lower q-values indicates that the sponge assemblies coexist with precursor-type objects, for instance folded vesicles (Figure 2, middle panel). They represent kinetically trapped long-lived intermediates of the vesicle-to-sponge nanoparticle transition.

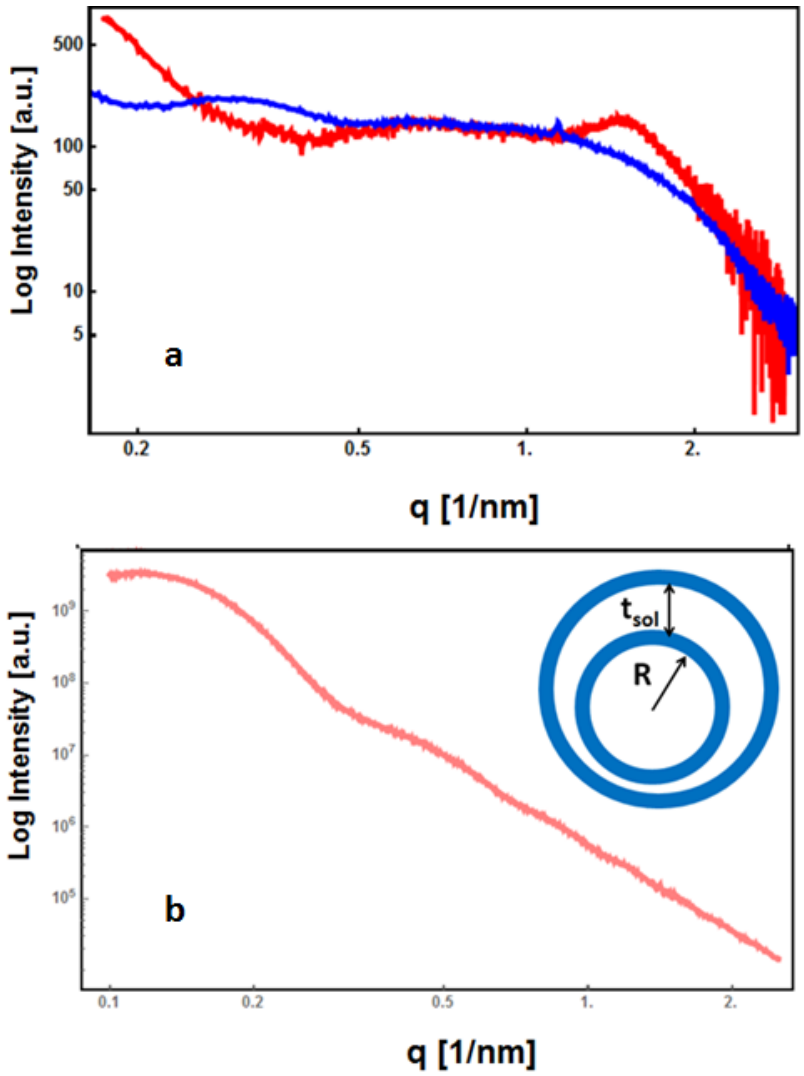

Figure 1. (a) Small-angle X-ray scattering (SAXS) patterns of diluted dispersions of monoolein-eicosapentaenoic acid assemblies (MO/EPA/DOPE-PEG_{2000} and MO/EPA/$TPGS_{1000}$) comprising 5 wt% lipid phase and 95 wt% water phase. The MO/EPA molar ratio is 85/15 (blue plot) and 30/70 mol/mol (red plot). The percentage of the PEGylated lipid is constant (3 mol.%) with regard to MO. Aqueous phase: 1.10^{-2} M phosphate buffer containing BHT. (b) Model SAXS curve fitted for random multilamellar vesicles involving two bilayers (double membrane vesicles), an inner radius *R,* and an intermembrane thickness of the aqueous buffer solvent, t_{sol}.

3.2. Cryo-TEM imaging revealing the proliferation of membrane linking pores (MLP) upon the vesicle-to-sponge nanoparticle transition

Experimental cryo-TEM data and a schematic model, characterizing the vesicle-to-sponge nanoparticle transition through the proliferation of membrane linking pores (MLP), are shown in Figure 2. The presented images demonstrate the development of sponge nanoparticle architectures of mixed compositions when the MO/EPA ratio changes from 85/15 (Fig. 2 left) to 30/70 (mol/mol) (Fig. 2 right) in the MO/EPA/DOPE-PEG_{2000} system. The lipid bilayers rearrange from spherical vesicles (Fig. 2 left) into 3D architectures of nanochannel topologies. This occurs through intermediate stages in a sequence of proliferation of pores. The density of the pores increases upon increase of the EPA fraction in the MO/EPA/DOPE-PEG_{2000} system (*i.e*. at MO/EPA ratio 30/70). In this sequence, the density of aqueous channels gets higher when the number of pores increases, respectively. Figure 2 (bottom panel) schematically presents a model of the transformation process of proliferation of pores. Correspondingly, the sizes of the aqueous channels decrease in the shown transition sequence. The insets present direct Fourier Transforms (FT) of (i) a cryoTEM image of the developed sponge organization and (ii) of the corresponding modeled pattern.

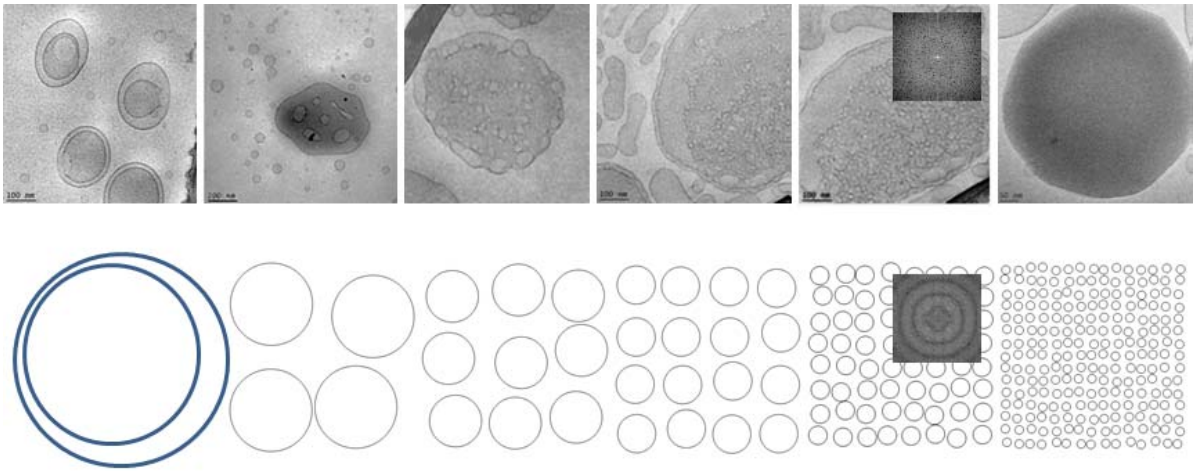

Figure 2. Vesicle-to-sponge nanoparticle transition through the proliferation of membrane linking pores (MLP). Top panel: Cryo-TEM images of dispersed vesicular and sponge lipid particles with different degrees of membrane perforation. The density of pores increases from left to right. The presented sequence of increasing density of aqueous channels (pores) demonstrates the stages of the vesicle-to-sponge transition. They comprise progressive perforation of the vesicle membranes into nanosponges of mixed compositions (middle), weakly hydrated spongosomes (right), and non-swollen (rich in EPA) particles of dense

inner organization (most right). The mixed MO/EPA/DOPE-PEG_{2000} assemblies (85/15 and 30/70 (mol/mol) ratios) are dispersed and stabilized using a DOPE-PEG_{2000} corona. The aqueous medium contains the antioxidant BHT ensuring the oxidative stability of the formulations. Bottom panel: Schematic modeling of the pathway of the vesicle-to-sponge transition *via* the proliferation of membrane-linking pores (top view of the MLPs). The insets represent the Fourier transforms (FT) of the corresponding Cryo-TEM image and the model pattern of MLP.

It is distinguishable in the images in Figure 2 (top panel) that the lipid bilayers fold upon the progression of the membrane perforation. The morphological change, associated with the membrane rearrangement, comprises nucleation of membrane linking pores (MLP). The latter generate ruptures of the lipid membranes. "Necks" are formed between the lipid bilayers as a demonstration of the occurring fluctuations of the curvature of the mixed lipid membranes. In the projected planes of the cryo-TEM images, the formation of the aqueous channels is observed as membrane pores (MLP) (Fig. 2, top panel). One observes a gradient of the distribution of pores from the center to the periphery of the lipid nanoparticles. The density of the pores varies because the dispersed objects can involve interfaces with uneven distributions of membrane curvature. This may be explained by differences in the composition distribution in the inner region of the particles as compared to their surface regions [29].

The tendency toward a formation of a 3D sponge phase is evident at increasing fractions of the ω-3 polyunsaturated fatty acid component. The degree of proliferation of the pores (*i.e.* the concentration of the MLP) augments with the increase of the EPA fraction. Thus, the topological transition occurs from a less perforated state to a more perforated state. The resulting texture of high density of pores (MLP) corresponds to weakly hydrated sponge membrane assemblies. The degree of hydration, respectively the sizes of the aqueous compartments, correlate with the fraction of incorporated PUFA in the mixed lipid membrane. It is evident that the ω-3 polyunsaturated fatty acid leads to swelling inhibition of the MO liquid crystalline structure as well as to more enhanced pore formation of the mixed membranes, which triggers a phase transition to a 3D sponge phase topology.

Regarding the effect of the PEGylated lipid added to the MO/EPA mixtures, it should be noted that the $TPGS_{1000}$ amphiphile resulted in a cauliflower nanoparticle topology (Fig. 3), whereas the double chain phospholipid DOPE-PEG_{2000} is involved in the formation of pored membrane architecture (Fig. 2). These differences require further structural studies of the lyotropic lipid polymorphism in these mixtures in order to better understand the involved interfacial curvature mechanisms.

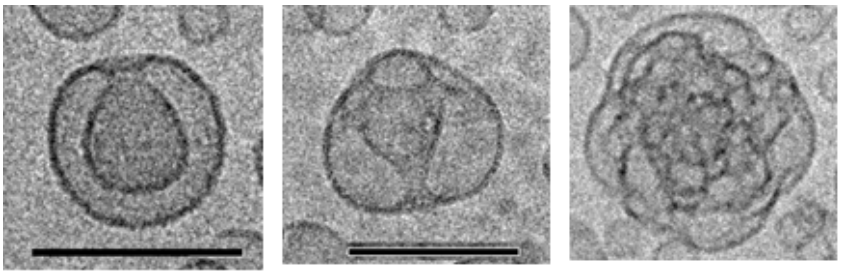

Figure 3. Cryo-TEM images showing a perforated vase-like double bilayer membrane vesicle (left), a folded vesicle (middle), and a sponge nanoparticle with a cauliflower inner membrane architecture of a in the self-assembled MO/EPA/$TPGS_{1000}$ dispersion system. The scale bar is 200 nm.

4. Conclusions

The performed investigations by synchrotron small-angle X-ray scattering (SAXS) and cryogenic transmission electron microscopy (Cryo-TEM) evidenced the intermediates of the vesicle-to-sponge transition that is triggered by composition variations in the self-assembled MO/EPA lipid mixtures. The dispersion of the four component liquid crystalline MO/EPA/DOPE-PEG_{2000}/water systems through sonication in excess aqueous phase was characterized by the formation of nano-objects with uneven distributions of the interfacial monolayer curvature. The presence of the ω-3 polyunsaturated fatty acid EPA (20:5) at high concentrations in the mixed assemblies provoked a higher density of membrane linking pores (MLP) and the formation of well-defined sponge particles (spongosomes). Swelling inhibition was established at increasing fraction of EPA in the mixed membranes, which corresponded to nanochannels of smaller sizes. Therefore, dehydration of the overall self-assembled sponge structure and a phase separation of the polyunsaturated fatty acid may be expected upon further increase of the EPA content.

Acknowledgement

The synchrotron SAXS data were collected at beamline P12 operated by EMBL Hamburg at the PETRA III storage ring of DESY (Deutsche Elektronen Synchrotron, Hamburg, Germany). We would like to thank C.E. Blanchet for the assistance in using the beamline. B.A. is supported by the project Structural dynamics of biomolecular systems (CZ.02.1.01/0.0/0.0/15_003/0000447) from European Regional Development Fund (ELIBIO), and the Czech Science Foundation project No.17-00973S. The results of the Project LQ1606 were obtained with the financial support of the Ministry of Education, Youth and Sports of Czech Republic as part of targeted support from the National Program of Sustainability II. M.D. is supported by the collaborative research centre SFB840 of the German Science Foundation DFG.

References

[1] S.T. Hyde, Identification of lyotropic liquid crystalline mesophases. In Handbook of Applied Surface and Colloid Chemistry; Holmberg, K., Ed.; John Wiley & Sons: Chichester, U.K., 2002; pp 299– 332.

[2] L. de Campo, A. Yaghmur, L. Sagalowicz, M.E. Leser, H. Watzke, O. Glatter, Reversible phase transitions in emulsified nanostructured lipid systems. Langmuir 20 (2004) 5254–5261.

[3] B. Angelov, A. Angelova, M. Drechsler, V.M. Garamus, R. Mutafchieva, S. Lesieur, Identification of large channels in cationic PEGylated cubosome nanoparticles by synchrotron radiation SAXS and Cryo-TEM imaging. Soft Matter 11 (2015) 3686–92.

[4] S. Aleandri, C. Speziale, R. Mezzenga, E.M. Landau, Design of light-triggered lyotropic liquid crystal mesophases and their application as molecular switches in "on demand" release, Langmuir 31 (2015) 6981-7.

[5] P. Wadsten, A.B. Wöhri, A. Snijder, G. Katona, A.T. Gardiner, R.J. Cogdell, R. Neutze, S. Engström, Lipidic Sponge Phase Crystallization of Membrane Proteins. J Mol Biol. 364 (2006) 44-53.

[6] C.E. Conn, C. Darmanin, X. Mulet, A. Hawley, C.J. Drummond, Effect of lipid architecture on cubic phase susceptibility to crystallisation screens. Soft Matter 8 (2012) 6884-6896.

[7] A. Angelova, B. Angelov, R. Mutafchieva, S. Lesieur, P. Couvreur, Self-assembled multicompartment liquid crystalline lipid carriers for protein, peptide, and nucleic acid drug delivery. Acc. Chem. Res. 44 (2011) 147– 156.

[8] V. Cherezov, E. Yamashita, W. Liu, M. Zhalnina, W.A. Cramer, M. Caffrey, *In meso* structure of the cobalamin transporter, BtuB, at 1.95 angstrom resolution, J. Mol. Biol. 364 (2006) 716–734.

[9] A. Angelova, V.M. Garamus, B. Angelov, Z. Tian, Y. Li, A. Zou, Advances in structural design of lipid-based nanoparticle carriers for delivery of macromolecular drugs, phytochemicals and anti-tumor agents. Adv. Colloid Interface Sci. 249 (2017) 331–345.

[10] L.P.B. Guerzoni, V. Nicolas, A. Angelova, *In vitro* modulation of TrkB receptor signaling upon sequential delivery of curcumin-DHA loaded carriers towards promoting neuronal survival. Pharm. Res. 34 (2017) 492–505.

[11] V. Cherezov and M. Caffrey, Membrane protein crystallization in lipidic mesophases. A mechanism study using X-ray microdiffraction, Faraday Discuss. 136 (2007) 195–212.

[12] R. Mezzenga, A. Zabara, I. Amar-Yuli, Tuning *in-meso*-crystallized lysozyme polymorphism by lyotropic liquid crystal symmetry, Langmuir 27 (2011) 6418–6425.

[13] A. Angelova, B. Angelov, M. Drechsler, V.M. Garamus, S. Lesieur, Protein entrapment in PEGylated lipid nanoparticles. Int. J. Pharm. 454 (2013) 625–632.

[14] Z. Almshergi, S. Hyde, M. Ramachandran, Y. Deng, Cubic membranes: a structure-based design for DNA uptake. J. R. Soc. Interface, 5 (2008) 1023-1029.

[15] A. Angelova, C. Fajolles, C. Hocquelet, F. Djedaıni-Pilard, S. Lesieur, R. Cortesi, Physico-chemical investigation of asymmetrical peptidolipidyl-cyclodextrins, Journal of Colloid and Interface Science, 322 (2008) 304-314.
[16] L. de Campo, T. Castle, S.T. Hyde, Optimal packings of three-arm star polyphiles: from tricontinuous to quasi-uniformly striped bicontinuous forms. Interface Focus. 7 (2017) 20160130.
[17] A. Angelova, J. Reiche, R. Ionov, D. Janietz, L. Brehmer, Control of the structure of Langmuir-Blodgett films of a discotic liquid crystalline compound via the subphase composition and the adjacent molecular environment, Thin Solid Films, 242 (1994) 289-294.
[18] A. Accardo, P. Ringhieri, N. Szekely, V. Pipich, A. Luchini, L. Paduano, D. Tesauro, Structural insights on nanoparticles containing gadolinium complexes as potential theranostic. Colloid Polym. Sci. 292 (2014) 1121–1127.
[19] G. Mangiapia, M. Vaccaro, G. D'Errico, H. Frielinghaus, A. Radulescu, V. Pipich, A.M. Carnerup, L. Paduano, Cubosomes for ruthenium complex delivery: formulation and characterization. Soft Matter 7 (2011) 10577–10580.
[20] X. Shao, G. Bor, S. Al-Hosayni, S. Salentinig, A. Yaghmur, Structural characterization of self-assemblies of new omega-3 lipids: docosahexaenoic acid and docosapentaenoic acid monoglycerides. Phys. Chem. Chem. Phys., 20 (2018) 23928-23941.
[21] S.P. Akhlaghi, I.R. Ribeiro, B.J. Boyd, W. Loh, Impact of preparation method and variables on the internal structure, morphology, and presence of liposomes in phytantriol-Pluronic(®) F127 cubosomes. Colloids Surf B. Biointerfaces 145 (2016) 845-853.
[22] B. Angelov, A. Angelova, S.K. Filippov, M. Drechsler, P. Štěpánek, S. Lesieur, Multicompartment lipid cubic nanoparticles with high protein upload: millisecond dynamics of formation. ACS Nano, 8 (2014) 5216–26.
[23] B. Angelov, A. Angelova, R. Mutafchieva, S. Lesieur, U. Vainio, V.M. Garamus, G.V. Jensen, J.S. Pedersen, SAXS investigation of a cubic to a sponge (L3) phase transition in self-assembled lipid nanocarriers. Phys. Chem. Chem. Phys. 13 (2011) 3073-3081.
[24] A. Yaghmur, B. Sartori, M. Rappolt, The role of calcium in membrane condensation and spontaneous curvature variations in model lipidic systems. Phys. Chem. Chem. Phys.13 (2011) 3115-3125.
[25] B. Angelov, V.M. Garamus, M. Drechsler, A. Angelova, Structural analysis of nanoparticulate carriers for encapsulation of macromolecular drugs. J. Mol. Liquids 235 (2017) 83–89.
[26] A. Yaghmur, P. Laggner,S. Zhang, M. Rappolt, Tuning Curvature and Stability of Monoolein Bilayers by Designer Lipid-Like Peptide Surfactants. PLoS One 2 (2007) e479.
[27] B. Angelov, A. Angelova, V.M. Garamus, G. Le Bas, S. Lesieur, M. Ollivon, S.S. Funari, R. Willumeit, P. Couvreur, Small-angle neutron and X-ray scattering from amphiphilic stimuli-responsive diamond-type bicontinuous cubic phase. J. Am. Chem. Soc., 129 (2007) 13474−13479.

[28] T. Lenné, C.J. Garvey, K.L. Koster, G. Bryant, Effects of Sugars on Lipid Bilayers during Dehydration - SAXS/WAXS Measurements and Quantitative Model. J. Phys. Chem. B 113 (2009) 2486–2491.
[29] M. Valldeperas, M. Wiśniewska, M. Ram-On, E. Kesselman, D. Danino, T. Nylander, J. Barauskas, Sponge phases and nanoparticle dispersions in aqueous mixtures of mono- and diglycerides. Langmuir 32 (2016) 8650-59.
[30] I.D.M. Azmi, J. Østergaard, S. Stürup, B. Gammelgaard, A. Urtti, S.M. Moghimi, A. Yaghmur, Cisplatin encapsulation generates morphologically different multicompartments in the internal nanostructures of nonlamellar liquid-crystalline self-assemblies. Langmuir 34 (2018) 6570–6581.
[31] A. Angelova, B. Angelov, B. Dual and multi-drug delivery nanoparticles towards neuronal survival and synaptic repair. Neural Regen. Res. 12 (2017) 886-889.
[32] L. Zerkoune, S. Lesieur, J.-L. Putaux, L. Choisnard, A. Gèze, D. Wouessidjewe, B. Angelov, C. Vebert-Nardin, J. Doutch, A. Angelova, Mesoporous self-assembled nanoparticles of biotransesterified cyclodextrins and nonlamellar lipids as carriers of water-insoluble substances. Soft Matter 12 (2016) 7539 - 7550.
[33] J. Barauskas, M. Johnsson, F. Tiberg, Self-assembled lipid superstructures: beyond vesicles and liposomes. Nano Lett. 5 (2005) 1615–1619.
[34] B. Klösgen, W. Helfrich, Special features of phosphatidylcholine vesicles as seen in cryo-transmission electron microscopy. Eur. Biophys. J. 22 (1993) 329-340.
[35] R. Efrat, E. Kesselman, A. Aserin, N. Garti, D. Danino, Solubilization of hydrophobic guest molecules in the monoolein discontinuous QL cubic mesophase and its soft nanoparticles. Langmuir 25 (2009) 1316-26.
[36] W.T. Góźdź, Cubosome topologies at various particle sizes and crystallographic symmetries. Langmuir 31 (2015) 13321-6.
[37] Y. Deng, Z.A. Almsherqi, G. Shui, M.R. Wenk, S.D. Kohlwein, Docosapentaenoic acid (DPA) is a critical determinant of cubic membrane formation in amoeba Chaos mitochondria. FASEB J. 23 (2009) 2866-71.
[38] C.V. Kulkarni, A. Yaghmur, M. Steinhart, M. Kriechbaum, M. Rappolt, Effects of high pressure on internally self-assembled lipid nanoparticles: A synchrotron small-angle X-ray scattering (SAXS) study. Langmuir 32 (2016) 11907-11917.
[39] A. Yaghmur, L. de Campo, L. Sagalowicz, M.E. Leser, O. Glatter, Control of the internal structure of MLO-based isasomes by the addition of diglycerol monooleate and soybean phosphatidylcholine. Langmuir 22 (2006) 9919-27.
[40] E. Nazaruk, M. Szlęzak,E. Górecka, R. Bilewicz, Y.M. Osornio, P. Uebelhart, E.M. Landau, Design and assembly of pH-sensitive lipidic cubic phase matrices for drug release. Langmuir 30 (2014) 1383–90.
[41] S. Aleandri, C. Speziale, R. Mezzenga, E.M. Landau, Design of light-triggered lyotropic liquid crystal mesophases and their application as molecular switches in 'On demand' release. Langmuir 31 (2015) 6981–6987.
[42] W.-K. Fong, A. Sánchez-Ferrer, F. G. Ortelli, W. Sun, B.J. Boyd, R. Mezzenga, Dynamic formation of nanostructured particles from vesicles via invertase hydrolysis for on-demand delivery, RSC Adv. 7 (2017) 4368-4377.

[43] X. Mulet, X. Gong, L.J. Waddington, C.J. Drummond, Observing Self-Assembled Lipid Nanoparticles Building Order and Complexity through Low-Energy Transformation Processes. ACS Nano 3 (2009) 2789–2797.
[44] A.S. Fogden, M. Stenkula, C.E. Fairhurst, M.C. Holmes, M.S. Leaver, Hexagonally perforated lamellae with uniform mean curvature. Progress in Colloid Polymer Sci. 108 (2008) 129-138.
[45] M. Gontsarik, M.T. Buhmann, A. Yaghmur, Q. Ren, K. Maniura-Weber, S. Salentinig, Antimicrobial Peptide-Driven Colloidal Transformations in Liquid-Crystalline Nanocarriers. J Phys Chem Lett. 7 (2016) 3482-6.
[46] A. Angelova, B. Angelov, B. Papahadjopoulos-Sternberg, M. Ollivon, C. Bourgaux, Structural organization of proteocubosome carriers involving medium- and large-size proteins. J Drug Deliv Sci Tech. 15 (2005) 108–112.
[47] K. Chong, Y. Deng, The three dimensionality of cell membranes: lamellar to cubic membrane transition as investigated by electron microscopy. Methods Cell Biol. 108 (2012) 317-43.
[48] C. Ge, J. Gómez-Llobregat, M.J. Skwark, J.M. Ruysschaert, A. Wieslander, M. Lindén, Membrane remodeling capacity of a vesicle-inducing glycosyltransferase. FEBS J. 281 (2014) 3667-84.
[49] N.C. Kegulian, S. Sankhagowit, M. Apostolidou, S.A. Jayasinghe, N. Malmstadt, P.C. Butler, R. Langen, Membrane Curvature-sensing and Curvature-inducing Activity of Islet Amyloid Polypeptide and Its Implications for Membrane Disruption. J Biol Chem. 290 (2015) 25782-93.
[50] Y. Chen, A. Angelova, B. Angelov, M. Drechsler, V.M. Garamus, R. Willumeit-Römer, A. Zou, Sterically stabilized spongosomes for multi-drug delivery of anticancer nanomedicines, J. Mater. Chem. B 3 (2015) 7734-7744.
[51] A. Zou, Y. Li, Y. Chen, A. Angelova, V.M. Garamus, N. Li, M. Drechsler, B. Angelov, Y. Gong, Self-assembled stable sponge-type nanocarries for *Brucea javanica* oil delivery. Colloids Surf. B: Biointerfaces 153 (2017) 310-319.
[52] R.Gomati, N.Bouguerra, A.Gharbi, Stability and swelling behaviour of a concentrated sponge phase. Physica B Condensed Matter 299 (2001) 101-107.
[53] R. Strey, R. Schomäcker, D. Roux, F. Nallet, U. Olsson, Dilute lamellar and L3 phases in the binary water-C12E5 system. J. Chem. Soc., Faraday Trans. 86 (1990) 2253-2261.
[54] H. Hoffmann, C.Thunig, U.Munkert, H.W. Meyer, W. Richter, From Vesicles to the L3 (Sponge) Phase in Alkyldimethylamine Oxide/Heptanol Systems. Langmuir, 8 (1992) 2629–2638.
[55] D. Roux, C.R. Safynia, A synchrotron X-ray study of competing undulation and electrostatic interlayer interactions in fluid multimembrane lyotropic phases. Journal de Physique, 49 (1998) 307–318.
[56] X. Michalet, D. Bensimon, B. Fourcade, Fluctuating vesicles of nonspherical topology. Phys Rev Lett. 72 (1994) 168–171.
[57] F. Jülicher, U. Seifert, R. Lipowsky, Conformal degeneracy and conformal diffusion of vesicles. Phys Rev Lett. 71 (1993) 452–455.

[58] C. Huang, D. Quinn, Y. Sadovsky, S. Suresh, K.J. Hsia, Formation and size distribution of self-assembled vesicles. Proc Natl Acad Sci U S A. 114 (2017) 2910-2915.
[59] B. Klösgen, W. Helfrich, Cryo-transmission electron microscopy of a superstructure of fluid dioleoylphosphatidylcholine (DOPC) membranes. Biophys J. 73 (1997) 3016–3029.
[60] S. Mahabir, D. Small, M. Li, W. Wan, N. Kučerka, K. Littrell, J. Katsaras, Mu-Ping Nieh, Growth kinetics of lipid-based nanodiscs to unilamellar vesicles—A time-resolved small angle neutron scattering (SANS) study. Biochimica et Biophysica Acta (BBA) - Biomembranes 1828 (2013) 1025-1035.
[61] R.P. Bradley, R. Radhakrishnan, Curvature-undulation coupling as a basis for curvature sensing and generation in bilayer membranes. Proc Natl Acad Sci U S A. 113 (2016) E5117-24.
[62] C.E. Conn, O. Ces, X. Mulet, S. Finet, R. Winter, J. M. Seddon, R. H. Templer, Dynamics of Structural Transformations between Lamellar and Inverse Bicontinuous Cubic Lyotropic Phases Phys. Rev. Lett. 96 (2006) 108102.
[63] N. Tran, J. Zhai C.E. Conn, X. Mulet, L.J. Waddington, C.J. Drummond, Direct Visualization of the Structural Transformation between the Lyotropic Liquid Crystalline Lamellar and Bicontinuous Cubic Mesophase. J Phys Chem Lett. 9 (2018) 3397-3402.
[64] R. Prajapati, S. Salentinig, A. Yaghmur, Temperature triggering of kinetically trapped self-assemblies in citrem-phospholipid nanoparticles, Chemistry Physics Lipids, 216 (2018) 30–38.
[65] A.I. Arwen, H.M.G. Barriga, E.S. Parsons, N L.C. McCarthy, O. Ces, R.V. Law, J.M. Seddon, N. J. Brooks, Electrostatic swelling of bicontinuous cubic lipid phases. Soft Matter 11 (2015) 3279-3286.
[66] S.E. Wilner, Q. Xiao, Z.T. Graber, S.E. Sherman, V. Percec, T. Baumgart, Dendrimersomes Exhibit Lamellar-to-Sponge Phase Transitions. Langmuir 34 (2018) 5527–5534.
[67] D.P. Siegel, J.L. Burns, M.H. Chestnut, Y.Talmon, Intermediates in membrane fusion and bilayer/nonbilayer phase transitions imaged by time-resolved cryo-transmission electron microscopy. Biophys J., 56 (1989) 161–169.
[68] N. Tran, X. Mulet, A. M. Hawley, C. Fong, J. Zhai, T.C. Le, J. Ratcliffe, C.J. Drummond, Manipulating the Ordered Nanostructure of Self-Assembled Monoolein and Phytantriol Nanoparticles with Unsaturated Fatty Acids. Langmuir 34 (2018) 2764-2773.
[69] I. Martiel, S. Handschin, W.-K. Fong, L. Sagalowicz, R. Mezzenga, Oil Transfer Converts Phosphatidylcholine Vesicles into Nonlamellar Lyotropic Liquid Crystalline Particles. Langmuir 31 (2015) 96-104.
[70] B. Angelov, A. Angelova, V.M. Garamus, M. Drechsler, R. Willumeit, R. Mutafchieva, P. Štěpánek, S. Lesieur, Earliest stage of the tetrahedral nanochannel formation in cubosome particles from unilamellar nanovesicles. Langmuir 28 (2012) 16647–55.
[71] B. Angelov, A. Angelova, U. Vainio, V.M. Garamus, S. Lesieur, R. Willumeit, P. Couvreur P. Long living intermediates during a lamellar to a diamond-cubic lipid phase

transition: A small-angle X-ray scattering investigation, Langmuir 25 (2009) 3734-3742.
[72] K. Tajima, M. Koshinuma, A. Nakamura, N.L. Gershfeld, Sponge-Vesicle Transformation in Binary Mixtures of Ionized Phospholipid Bilayers. Langmuir 16 (2000) 2576– 2580.
[73] Noguchi H., Shape transitions of high-genus fluid vesicles, EPL 112 (2015) 58004.
[74] K.-i. Akashi, H. Miyata, Lipid bilayer vesicles with numbers of membrane linking pores, J. Phys. Soc. Jpn. 79 (2010) 064801.
[75] S. J. Marrink, A.H. de Vries, D.P. Tieleman, Lipids on the move: Simulations of membrane pores, domains, stalks and curves. Biochimica et Biophysica Acta (BBA) - Biomembranes 1788 (2009) 149-168.
[76] C.E. Blanchet, A. Spilotros, F. Schwemmer, M.A. Graewert, A.G. Kikhney, C.M. Jeffries, D. Franke, D. Mark, R. Zengerle, F. Cipriani, S. Fiedler, M. Roessle, D.I. Svergun, Versatile sample environments and automation for biological solution X-ray scattering experiments at the P12 beamline (PETRA III, DESY). J. Appl. Cryst. 48 (2015) 431–443.
[77] P.V. Konarev, V.V. Volkov, A.V. Sokolova, M.H.J. Koch, D. I. Svergun . PRIMUS - a Windows-PC based system for small-angle scattering data analysis. J Appl Cryst. 36 (2003) 1277-1282.
[78] I. Breßler, J. Kohlbrecher, A.F. Thünemann, SASfit: a tool for small-angle scattering data analysis using a library of analytical expressions, J Appl Crystallogr. 48 (2015) 1587–1598.